Theor Chem Acc (2006) 116: 169–182
DOI 10.1007/s00214-005-0018-8

REGULAR ARTICLE

Shawn M. Kathmann

Understanding the chemical physics of nucleation

Received: 31 March 2005 / Accepted: 28 July 2005 / Published online: 15 December 2005

Abstract Observation and theory have steadily progressed our understanding of nucleation phenomena over the past 280 years. However, even more questions remain concerning the governing processes and mechanisms. The inherent instability and sensitivity of nucleation places a high premium on theoretical accuracy and experimental purity and similarly makes interpretation of both more challenging. The objective of the present paper is to contribute to the understanding of nucleation kinetics and thermodynamics with emphasis on cluster chemical physics within the context of Dynamical Nucleation Theory. Our hope is to share some insights that we have gained over the past several years concerning rate constants, molecular interactions, statistical mechanics and their consequences on nucleation.

1 Introduction

A phase transformation begins with the development of a supersaturated state resulting from a change in chemistry, temperature, pressure, or other physical condition (e.g., electromagnetic fields, acoustic waves, etc.). The supersaturated state generates clusters (or nuclei) of the new phase. These clusters can form homogeneously within the mother phase or heterogeneously on seeds, impurities, dust, ions, or other irregularities that provide the clusters with local regions of stability (e.g., defects, steps, edges, or other imperfections). Once these clusters reach a critical size, a favorable fluctuation allows them to grow to macroscopic dimension. Growth will continue until relaxation processes dominate resulting in the completion of the transformation.

Nucleation research has a long history spanning over 280 years (see Table 1) [1–17]. It began in 1724, when Farenheit [1] first studied freezing and phase equilibria to devise his temperature scale and was the first to investigate the supercooling of water. Many scientists continued to study nucleation and some highlights are worth mentioning here. Lowitz [2] observed that supersaturated solutions seeded with crystals of the new phase caused crystallization but that foreign seeds had no effect. In 1813, Gay-Lussac [4] studied how different chemical systems sustain different supersaturations before crystallizing and also found scratching, shaking, or rubbing could induce crystallization. In 1848, Pasteur [5] found that sodium ammonium tartrate (SAT) crystallized into a racemic mixture that ultimately led to the discovery of enantiomers (see Fig. 1) by separating the left (L) and right (R) handed crystals using tweezers. In 1866, Gernez [6] found that pure L or R SAT seed crystals did not crystallize a liquid of either R or L SAT, respectively. But, he [18] did find that isomorphous seed salts would (e.g., a $ZnSO_4 \cdot 7H_2O$ seed induces crystallization in $FeSO_4 \cdot 7H_2O$). In 1876, Gibbs [7] established the criterion for phase stability and derived the critical free energy of formation. Coulier [8], Aitken [9], and Wilson [10] found that droplet formation from normal air was sensitive to dust, ions, or other impurities. In 1889, Arrhenius [19] proposed a general relationship for the temperature dependence of reaction rates thus developing the concept of an activation barrier. In 1896, Ostwald [11] proposed the "Law of Stages". He [20] also tried to address the question "What is the smallest seed crystal required to induce nucleation?" by finding that for sodium chlorate ($NaClO_3$) only 10^{-10} g were needed (this amount corresponds to a seed of about 3.4 μm, i.e. barely visible under a microscope, containing about 6×10^{11} $NaClO_3$ molecules). In 1926, Volmer and Weber [12, 13] established a kinetic theory of nucleation and recognized that the metastability of the supersaturated state is a matter of kinetics—the frequency of critical cluster formation is proportional to the Boltzmann weight of the work of cluster formation—very similar to the Arrhenius activation theory. In 1927, Farkas [14] proposed a detailed kinetic mechanism whereby clusters grow and decay by addition and loss of single monomers and that the critical cluster, defined as that cluster for which the evaporation and condensation rates are equal, constitutes the bottleneck for the phase transformation. In 1935–1939, Becker and Döring [15], Band [16], and Frenkel [17] formulated classical nucleation theory (CNT) where the critical

S. M. Kathmann
Chemical Sciences Division, Pacific Northwest National Laboratory, Richland, WA 99352, USA
E-mail: shawn.kathmann@pnl.gov

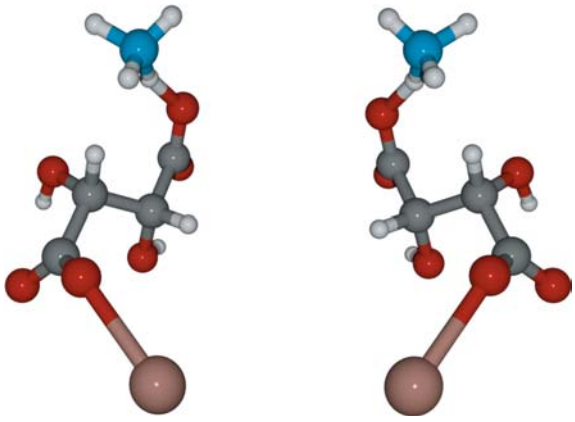

Fig. 1 Louis Pasteur discovered the existence of enantiomers using the crystallization of sodium ammonium tartrate (SAT): left (−) S,S-SAT and right (+) R,R-SAT

cluster is treated as a well-defined tiny nucleus of the new phase. CNT yields a steady state nucleation rate that is proportional to the collision rate of monomers onto the critical cluster multiplied by the concentration of critical clusters. Currently, CNT is the most widely used theoretical description to obtain nucleation rates, as it only requires the bulk surface tension (or interfacial free energy) and density of the nucleating substance.

In recent years, there have been extraordinary advances in experimental methodologies [21,22] to probe the small scales relevant to phase transformations, however, there remains a gap in theory, modeling, and simulation of nucleation. Significant advances have been made in theoretical and numerical methods that parallel and rival experimental advances but have yet to be fully exploited to understand the chemical physics of nucleation. The specific gaps in nucleation are the interaction potentials, thermodynamics, mechanisms, influence of solvent properties and/or impurities, and kinetic properties of all the clusters leading up to the critical size. In crystallization, if the concentration of a solution is gradually increased, exceeding the equilibrium solubility, a new crystal phase will not be formed within a specific amount of time until a critical supersaturation has been attained. The reason for this is because nucleation is a rare event process. Consequently, a solution that is just slightly supersaturated will not yield crystals because the probability of observing such crystals is vanishingly small given a reasonable amount of time and quantity (volume) of solution. Stable crystals will only form after a sufficient number of clusters have surmounted the activation barrier. Small perturbations in the interactions and conditions of nucleation can lead to qualitatively different critical embryo structures and alter the growth trajectory. Crystal surfaces develop in response to anisotropy in attachment/detachment kinetics and can be greatly influenced by the underlying bulk structure. The origins of particular growth patterns (dendrites, rods, etc.) and instabilities were discussed in the seminal work of Mullins and Sekerka [23,24]; the Mullins-Sekerka instability is initiated as the solidification front starts to propagate. The latent heat of solidification generated at the solid liquid interface must be conducted away from the interface in order for the crystal to grow. Propagation of a planar front into the metastable state (undercooled liquid) is intrinsically unstable—the front breaks up into many dendrite [24]. Another key feature of crystal growth is the Berg effect, which predicts that the growth of dendrites is highly favored in regions of higher supersaturation; the morphological instability at the growth start is due to a non-uniform supersaturation over the seed surface. Accordingly the supersaturation is higher at the edges of a finite crystal [25]. A good introduction to crystal growth is the review article by Langer [26] and further detailed thermodynamic derivations found in a book chapter by Caroli et al. [27].

This sensitivity leads to significant variations in collective structures and properties. Thus, in the long term it will be necessary to characterize and understand the limitations and uncertainties in the description of interactions, transport, and non-equilibrium effects. The demands on accuracy will push the limits of current knowledge and computational algorithms. Experimental studies have clearly demonstrated that nucleation is incredibly sensitive to the physical conditions including temperature, concentrations of nucleating species, light, sound, electromagnetic fields, transport, and the presence of trace impurities [8–10,12,28]. For example, Alivisatos and co-workers [29] have created Cadmium Telluride nano-tetrapods by utilizing the energy difference between the zinc-blende and wurtzite structures—the add-atom energy difference for these two structures is less than 0.1 kcal/mol.

The extreme sensitivity of nucleation to conditions calls for theoretical studies to provide a fundamental understanding the nature of the underlying molecular processes. A common question is "since nucleation is so sensitive can theoretical studies really improve our understanding?" The short answer is yes. Theory plays an essential role because the subtleties and nuances of the molecular processes governing nucleation cannot yet be experimentally ascertained—observation is limited. Through theoretical investigation the gaps in our knowledge can be bridged and mechanisms deduced while validating our theories with the latest experiments. We envision that future research into the chemical physics nucleation will allow this high degree of sensitivity to be exploited to exert extreme control over nucleation.

The paper is outlined as follows: (1) A brief review of Classical Nucleation Theory will be provided, (2) a description of recent molecular theories will be given, (3) Dynamical Nucleation Theory will be highlighted, and (4) applied to the homogeneous nucleation of water. In Sect. 5, Dynamical Nucleation Theory is extended to the simple case of two ions in solution. Section 6 is comments and conclusions.

2 Classical nucleation theory

Nucleation of the new phase requires surmounting an activation barrier via rare event processes. Using water as an

Table 1 Chronology of scientists and their developments toward understanding nucleation

Year	Scientist(s)	Development
1724	Fahrenheit	Studied freezing and phase equilibria to devise his temperature scale and was the first to supercool water.
1795	Lowitz	Observed that supersaturated solutions seeded with crystals of the new phase caused crystallization but that foreign seeds had no effect.
1806	Laplace	Derived the mathematical condition for mechanical equilibrium of a spherical droplet.
1813	Gay-Lussac	Studied how different chemical systems sustain different supersaturations before crystallizing and also found scratching, shaking, or rubbing could induce crystallization.
1848	Pasteur	Discovered enantiomers via crystallization of sodium ammonium tartrate (SAT).
1866	Gernez	Found that pure (L) or (R) SAT seed crystals did not crystallize a liquid of the opposite chirality.
1876	Gibbs	Established the criterion for phase stability and derived the critical free energy of formation.
1875	Coulier	
1880	Aitken	Found that droplet formation from normal air was sensitive to dust, ions, or other impurities.
1897	Wilson	
1886	Helmholtz	Found that droplet formation from a water vapor jet into air was sensitive to dust, ions, and other chemicals.
1896	Ostwald	Proposed the "Law of Stages" which states that a metastable supersaturated state does not spontaneously transform into the most stable state, but to the next state more stable than itself.
1926	Volmer and Weber	Established a kinetic theory of nucleation and recognized that the metastability of the supersaturated state is a matter of kinetics
1927	Farkas	Proposed a detailed kinetic mechanism whereby clusters grow and decay by addition and loss of single monomers and that the critical cluster constitutes the bottleneck for the phase transformation.
1935	Becker and Döring	
1939	Band	Formulated classical nucleation theory
1939	Frenkel	

example, the nucleation mechanism is described by condensation and evaporation of monomers

$$H_2O + (H_2O)_{i-1} \underset{\alpha_i}{\overset{\beta_{i-1}}{\rightleftharpoons}} (H_2O)_i \tag{1}$$

where β_{i-1} is the condensation rate constant for addition of a water molecule to a cluster, and α_i the evaporation rate constant for loss of a water molecule from a cluster. Using detailed balance, the ratio of evaporation and condensation rate constants is related to the ratio of equilibrium populations of adjacent cluster sizes, $N_i^{\mathrm{EQ}}/N_{i-1}^{\mathrm{EQ}}$, and equilibrium constants, $\mathrm{K}_{i-1,1}^{\mathrm{EQ}}$, by

$$\frac{\beta_{i-1}}{\alpha_{i-1}} = \frac{N_i^{\mathrm{EQ}}}{N_{i-1}^{\mathrm{EQ}}} = \mathrm{K}_{i-1,i}^{\mathrm{EQ}}. \tag{2}$$

The current, J_{i-1}, between adjacent clusters is given by

$$J_{i-1} = \beta_{i-1} N_{i-1} - \alpha_i N_i. \tag{3}$$

Under steady-state conditions ($\mathrm{d}N_i/\mathrm{d}t = J_{i-1} - J_i = 0$) the currents are all equal to a single current

$$J_{\mathrm{ss}} = \left[\sum_{i=1}^{\infty} \left(\beta_i N_i^{\mathrm{EQ}} \right)^{-1} \right]^{-1}. \tag{4}$$

If the above sum is treated as an integral and the maximum approximated by a Taylor expansion, then the familiar expression for the steady-state Becker-Döring nucleation rate is obtained by

$$J_{\mathrm{CNT}} \approx Z_{i^*} \beta_{i^*} N_{i^*}, \tag{5}$$

where Z_{i^*} is the Zeldovich [30] factor which accounts for the curvature of the nucleation barrier in the region of the critical cluster, β_{i^*} is the condensation rate onto the critical cluster (assumed to be the gas-kinetic collision rate), and N_i^* is the concentration of critical clusters and is given by

$$N_{i^*} = N_1 \exp\left[-W(i^*)/k_{\mathrm{B}}T \right], \tag{6}$$

where N_1 is the monomer concentration, $W(i^*)$ is the cluster work of formation or nucleation barrier, k_{B} is Boltzmann's constant, and T is the temperature. The critical cluster, as mentioned previously, is the cluster for which the evaporation and condensation rates are equal and coincident with the location of the peak in the nucleation barrier, $W(i^*)$, as shown in Fig. 2. The cluster work of formation is approximated as the formation of a liquid droplet given by

$$W(i) = -ik_{\mathrm{B}}T \ln S + 4\pi r_i^2 \sigma, \tag{7}$$

where S is the supersaturation defined as the ratio of ambient to equilibrium vapor pressure, r_i is the radius of the i-cluster as determined from the bulk liquid density ρ, and σ is the bulk liquid surface tension. The work of formation for the critical cluster is given by

$$W(i^*) = \frac{4\pi r_{i^*}^2 \sigma}{3} = \frac{16\pi\sigma^3}{3\rho^2 (k_{\mathrm{B}}T \ln S)^2}. \tag{8}$$

Using this quantity for the classical critical work of formation with Eqs. 5 and 6 and the Zeldovich factor yields

$$J_{\mathrm{CNT}} \approx \sqrt{\frac{2\sigma}{\pi m}} v_1 N_1^2 \exp\left[-\frac{16\pi\sigma^3}{3k_{\mathrm{B}}T\rho^2 (k_{\mathrm{B}}T \ln S)^2} \right], \tag{9}$$

where v_1 is the monomer volume, and m is the monomer mass. It should be clear from Eq. 9 that the nucleation rate depends strongly on the surface tension σ, meaning that small changes in this parameter can lead to large changes in the nucleation rate. CNT is a phenomenological model and if agreement between experiment and theory is observed, it is usually only within a narrow range of supersaturations and

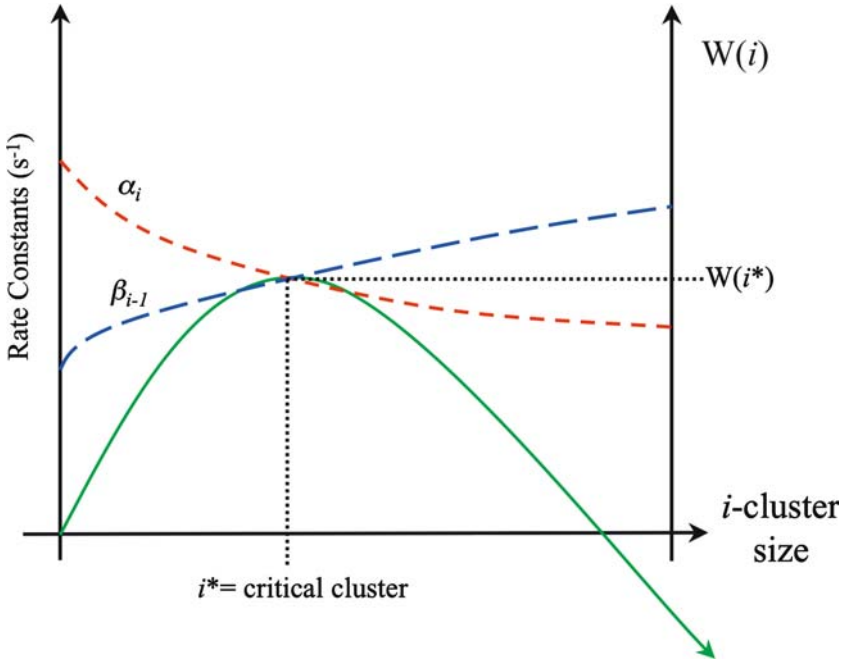

Fig. 2 The critical cluster (i^*) is defined the cluster for which the evaporation α_i and condensation β_{i-1} rate constants are equal. This occurs at the maximum in the nucleation barrier, W(i^*)

temperatures. Although many insights concerning nucleation have been obtained via CNT, it does not explicitly treat cluster chemical physics. At this point it becomes necessary to ask some fundamental questions: Is it appropriate to treat the small molecular clusters, which control the nucleation rate, like tiny droplets with bulk properties? How do the individual interactions between molecules influence the nucleation rate? How does one deal with trace ions, impurities, contaminants, etc.? What if the critical cluster is not spherical, how do we treat the interfacial free energy? The answer to all these questions must reside in the chemical physics of nucleating clusters, including treatment of trace species that can reduce the activation barrier and consequently increase the nucleation rate.

Recent work by Kulmala and coworkers [31], employing CNT on ternary nucleation of sulfuric acid (sulfuric acid concentrations ranging from 10^4 to 10^{10} cm^{-3}), ammonia, and water (RH = 90%), found that 25 ppt of ammonia increases the nucleation rate by nearly 20 orders of magnitude! Moreover, they found that the largest influence on the nucleation rate (the first 16 of the 20 orders of magnitude) occurs for ammonia concentrations below 5–4 ppt, which is currently the detection limit for ammonia measurements. This sensitivity lies in the variation in the surface tension when ammonia is added. Given the dubious validity of using surface tension to treat molecular clusters in the first place, the sensitivity that Kulmala and coworkers found provides further impetus to address the problem at the molecular level (e.g., the critical cluster they inferred from their calculations is comprised of 8 H_2SO_4, 7 H_2O, and 5 NH_3 molecules). Kulmala et al. [32] have concluded, based upon over 100 field measurements, that nucleation can lead to a significant increase in the number concentration of cloud condensation nuclei and thus global climate models must require reliable models for nucleation. All experimental conditions can be characterized by some amount of contamination and thus it is crucial to understand the underlying molecular processes if we are to interpret measurements of the nucleation rate. Unfortunately, it has become commonplace for nucleation researchers to attribute failures of CNT when compared to measurements (usually for multi-component systems) to some unaccounted for chemical component (e.g., organics, ions, etc.)—never appreciating that the theory is inadequate at the outset because it does not treat cluster chemical physics properly and that, in reality, nucleation is sensitive to the interactions between the species undergoing the phase transformation.

3 Molecular-based nucleation theories

The relatively small size of critical clusters (tens to hundreds of molecules) provides a compelling argument for treating molecules explicitly in the nucleation process. Promising alternatives to CNT employ molecular simulations [33, 34] in order to calculate cluster properties, which can then be used to determine nucleation rates [35–43]. Many of these molecular approaches take a similar view as CNT, approaching nucleation from a liquid-phase perspective, assuming condensation rate constants to be approximated by gas-phase collision rates with molecular droplets. The cluster distribution functions are obtained using molecular simulations to compute the relevant partition functions or Helmholtz free energies for the clusters. [35, 37, 44] However, before a molecular simulation can be performed the "*cluster*" must be defined. Most

previous molecular theories [35,45,46] have defined a cluster to be a collection of i molecules whose center of mass lies at the center of the spherical constraining shell. Furthermore, the Helmholtz free energy of the i-cluster was assumed to be independent of the constraining radius. The "correct" cluster volume and Helmholtz free energy to use in the cluster distribution function has been a source of confusion and controversy for almost 40 years [38,47]. Other molecular cluster approaches [43] use a Stillinger [48] connectivity definition—molecules closer than some preset value are defined as a cluster. Some molecular approaches [49] have attempted to directly observe the nucleation event by brute force simulation of a supersaturated vapor while employing the Stillinger cluster criterion. The conditions required to observe a nucleation event in these relatively small systems are typically beyond those amenable to experimental confirmation (e.g., at T = 350 K and a supersaturation of 7.3 yields a nucleation rate of ca. 10^{27} no./cc/s). Morever, these efforts are more simulative experiments rather than exact rate theories.

Alternatively, thermodynamic density functional theory (DFT) has been used to calculate the free energy barrier to nucleation [50]. DFT provides a rigorous statistical mechanical means of determining the thermodynamic properties of inhomogeneous system starting from an intermolecular potential but without calculating the partition function. The critical cluster is obtained by finding the density profile that minimizes the system Helmholtz free energy. However, this benefit may be sacrificed by approximating the true intermolecular potential with hard-sphere perturbation theory in addition to not sampling the full anharmonic partition function. Although great promise has been shown by these approaches, until recently they have been applied primarily to model systems (e.g., using spherically symmetric Lennard-Jones and Yukawa potentials). Furthermore, attention has not been focused on the sensitivity of the critical cluster properties to the interaction energies or the role of classical versus quantum statistical mechanics (i.e., quantum nuclear degrees of freedom) or the individual mechanisms, thermodynamics, and kinetics of the pre-critical clusters.

We also note that dynamical nucleation theory (DNT) has some similarity to the method of ten Wolde and Frenkel [51,52] who have applied transition state theory (TST) to nucleation in a model Lennard-Jones system. In DNT we calculate the rate constants for evaporation and condensation for each i-cluster using Variational TST (VTST), whereas ten Wolde and Frenkel have formulated the nucleation rate in terms of TST where the rate of critical cluster formation is determined by umbrella sampling the critical clusters and analyzing dynamical trajectories about the critical region. The key similarity between DNT and the ten Wolde-Frenkel formalism is the use of TST. But, the way TST is used and for which clusters it is applied are different. In particular, the ten Wolde-Frenkel formalism uses the cluster size as the reaction coordinate (a local order parameter with a cluster defined by Stillinger-like connectivity requirements), umbrella samples the critical cluster work of formation using Monte Carlo (MC), and computes the transition rate and transmission factor (to account for dynamical re-crossing effects) using molecular dynamics (MD) trajectories evolved from phase space points obtained during the MC umbrella sampling of critical clusters. In DNT, we compute the evaporation rate constant for *each* i-cluster where the relevant cluster configuration space defined by a variational procedure that minimizes the evaporative reactive flux. Using the VTST procedure, the best estimates for the classical evaporation rate constants are obtained using MC simulations, Helmholtz free energy differences between adjacent-sized clusters calculated from MC simulations, condensation rate constants determined via detailed balance, and total nucleation rates calculated by solving resulting kinetics equations. Additional explicit MD simulations can be performed to quantify re-crossing effects. Thus, DNT provides a means to obtain evaporation rate constants for all clusters involved in the nucleation process and a cluster definition based on those that are most stable with respect to evaporation (more details are provided below in the section on DNT). It will be interesting to make more definitive comparisons of the two approaches in the future.

For the current paper, our focus is on DNT and the associated cluster chemical physics. Professor Howard Reiss [53] has written a valuable review in his "Critique of Molecular Theories of Nucleation". In clear support of DNT, he writes "... among the several developing molecular theories of [nucleation] rate that can be compared to assess the validity of all of them, the interesting approach of Garrett and coworkers, who are developing a theory based upon variational transition state theory, must be included." We hope to share some insights that we have gained over the past several years concerning rate constants, interactions, statistical mechanics and their consequences on nucleation.

4 Dynamical nucleation theory

A novel exception to previous molecular approaches is DNT [36,40–42,54–57]. DNT is a molecular-level approach, recently developed for the study of homogeneous vapor-phase nucleation. DNT utilizes a gas-phase reaction kinetics perspective and thus provides a natural setting in which the kinetic parameters and rate constants, necessary for the construction of a consistent nucleation theory, can be obtained. In DNT, as in CNT, nucleation is treated via monomer condensation and evaporation reaction channels (see Eq. 1). The emphasis of DNT is on the evaluation of monomer evaporation rate constants from clusters. As in other molecular approaches the cluster Helmholtz free energy is an important quantity as it determines the cluster population. DNT does not require bulk thermodynamic properties such as the liquid density, surface tension, or vapor pressures. Using the mathematical framework of DNT, systematically improvable nucleation models for multi-component systems can be created employing a fundamentally sound description of the thermodynamic and kinetic properties of clusters relevant to nucleation. These models could provide a framework in

which increasingly more accurate calculations on clusters can be readily incorporated. This aspect of DNT was noted by Heneghan et al. [58] who stated "As better and better intermolecular potentials are developed, this method [DNT] will become more and more applicable."

Significant progress has been made in developing DNT over the last few years and these advances provide the basis for a true molecular-level understanding of nucleation. A brief summary of the advances are provided here.

- An expression for the evaporation rate constant was *directly* obtained by using variational transition state theory with a spherical dividing surface centered on the center of mass of the cluster. The surprising result is that the evaporation rate constant is proportional to the derivative of the Helmholtz free energy for cluster formation with respect to the radius of the spherical dividing surface [40].
- The optimum value of the constraining radius is uniquely determined by the variational criteria of VTST, which minimizes the rate constant. Therefore, DNT provides the first physically justified procedure for selecting a unique volume for an *i*-cluster, which as mentioned above has been a source of controversy in the literature. This volume is physically justified because it defines the clusters that are most stable (i.e., with the slowest rate) to evaporation.
- A consistent theoretical approach was provided for calculating the condensation rate constants using detailed balance and equilibrium constants that are consistent with the evaporation rate constants. It is important to note that in this approach, the condensation rate constants are determined *directly* without assuming the condensation rate is given by the gas-kinetic collision rate [59].
- The formalism has been extended to nucleation involving multiple components [56].
- Computational methods were developed to calculate (1) the dependence of the Helmholtz free energy of cluster formation on the radius of the constraining volume, which is needed to determine the evaporation rate constants, and (2) the relative differences in Helmholtz free energies for clusters of different sizes, which are needed for the equilibrium constants and condensation rate constants [59].
- Accurate dynamical simulations of the reaction dynamics were performed calibrating the accuracy of VTST for the evaporation and condensation rate constants [41].
- Sensitivity studies of the nucleation kinetics were implemented for multi-component systems (for the first time). These studies indicated the most computationally efficient procedures for calculating the parameters needed to obtain nucleation rates [56].
- An extreme sensitivity of the kinetic parameters, and thereby the nucleation rates, to the underlying interaction potentials has been discovered in addition to classical versus quantum statistical mechanical effects (zero-point-energies) used in the molecular simulations. These results indicate the extreme sensitivity of nucleation experiments to possible contaminants, since trace species in a small molecular cluster can significantly alter the molecular interactions [55].
- Calculations on ion-water clusters show that specification of the ion's charge and sign alone are insufficient to provide an understanding of cluster thermodynamics and that classical ion-induced nucleation theory does not treat the cluster physics properly to describe ion-induced nucleation [57].

The details of DNT have been addressed in previous publications and only the essential concepts will be addressed here. In DNT, the ambiguity in defining the cluster is removed through application of VTST. For each evaporation event, the dynamical bottleneck in phase space is explicitly evaluated. This bottleneck corresponds to a dividing surface in phase space separating reactant (the i cluster) and product (the $i-1$ cluster plus a monomer separated at infinity) regions. From this dividing surface an unambiguous definition of the cluster emerges which is consistent with detailed balance. The initial formulation of DNT assumed a spherical dividing surface whose origin is placed at the cluster center-of-mass with the constraining radius of the sphere denoted as r_{cut} (see Fig. 3). This choice of dividing surface results in an expression for the monomer evaporation rate constant, α_i, given by

$$\alpha_i(r_{\mathrm{DNT}}, T) = -\frac{1}{\sqrt{2\pi m k_{\mathrm{B}} T}} \left.\frac{dA_i(r_{\mathrm{cut}}, T)}{dr_{\mathrm{cut}}}\right|_{r_{\mathrm{cut}}=r_{\mathrm{DNT}},} \tag{10}$$

where m is the mass of the water monomer, A_i is the i-cluster Helmholtz free energy, and r_{DNT} is the value of the constraining radius that variationally minimizes the reactive flux through the dividing surface. Equation 10 can be expressed in a form similar to the gas-kinetic collision rate by

$$\alpha_i\left(r_{\mathrm{DNT}}, T\right) = \frac{\bar{c}}{4}\left(4\pi r_{\mathrm{DNT}}^2\right)\frac{p_i^{\mathrm{int}}(r_{\mathrm{DNT}}, T)}{k_{\mathrm{B}} T}, \tag{11}$$

where the mean speed $\bar{c} = \sqrt{8k_{\mathrm{B}}T/\pi m}$, and the cluster internal pressure is given by

$$p_i^{\mathrm{int}}\left(r_{\mathrm{DNT}}, T\right) \equiv -\left.\frac{dA_i(r_{\mathrm{cut}}, T)}{dv_i}\right|_{r_{\mathrm{cut}}=r_{\mathrm{DNT}},} \tag{12}$$

where v_i is the i-cluster volume.

Dynamical nucleation theory provides a significant advantage since the estimate of the evaporation rate constant can be systematically improved through consideration of increasingly more general dividing surfaces. Since the nature of the chosen dividing surface separating reactant and product regions of phase space can have a profound influence on the validity and accuracy of the rate estimation, we have benchmarked our spherical dividing surface against explicit dynamics [41] calculations on water clusters at 243 K and found dynamical corrections (transmission factors) of approximately a factor of two. The reason for choosing a spherical dividing surface was to make connection with previous statistical mechanical approaches to nucleation [45,60]. The dividing surface is defined by the relation $\mathrm{S}(\mathbf{r}^i) = 0$, where

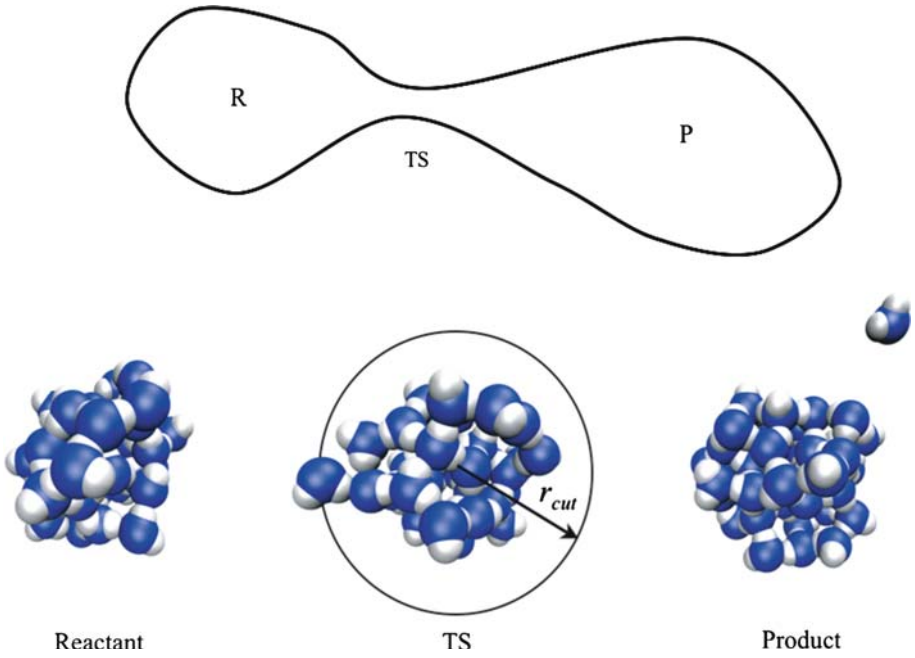

Fig. 3 Conceptual illustration of phase space partitioning used in dynamical nucleation theory (DNT). Reactant region (R) = i-cluster, transition state (TS) = i-cluster with a monomer lying on the dividing surface, product region (P) = $i-1$ cluster plus a monomer located outside constraining sphere

$\mathbf{r}^i$ denotes the set of all position coordinates. For the spherical dividing surface, $S(\mathbf{r}^i)$ is given by

$$S(\mathbf{r}^i) = \max_k \left| \mathbf{r}_k - \frac{1}{i}\sum_{j=1}^{i} \mathbf{r}_j \right| - r_{\text{cut}}, \tag{13}$$

where k denotes one of the molecules in the cluster. When $S(\mathbf{r}^i) < 0$, the cluster is in the reactant region of phase space with all molecules lying within the constraining sphere of radius r_{cut}. When $S(\mathbf{r}^i) > 0$, at least one molecule is outside the constraining sphere and the cluster is considered to be in the product region of phase space. The i-cluster anharmonic canonical partition function (with center-of-mass translation removed) is given by

$$q_i(v, T) = \frac{\gamma^i}{i!} \int \mathrm{d}\mathbf{r}^i \exp\left[-U(\mathbf{r}^i)/k_{\text{B}}T\right] \Theta\left[-S(\mathbf{r}^i)\right], \tag{14}$$

where $\gamma = (2\pi m k_{\text{B}}T/h^2)^{3/2}$, h is Planck's constant, and $U(\mathbf{r}^i)$ is the interaction potential. The constraining sphere Θ given by

$$\Theta\left[-S\left(\mathbf{r}^i\right)\right] = \prod_{j=1}^{i} \theta\left(r_{\text{cut}} - \left|\mathbf{r}_j - \mathbf{R}_i\right|\right), \tag{15}$$

where $\theta(\mathrm{x})$ is the Heaviside step function, and $\mathbf{R}_i$ is the cluster center-of-mass. The i-cluster anharmonic Helmholtz free energy is

$$A_i(v, T) = -k_{\text{B}}T \ln\left[q_i\left(v, T\right)\right]. \tag{16}$$

We illustrate the results for obtaining the evaporation rate constant for the Dang-Chang [61] water dimer at 243 K in Fig. 4 (note that the evaporation rates are independent of supersaturation). In Fig. 4, the lower graph shows the constraining radius dependence of the Helmholtz free energy and how for large r_{cut} the free energy approaches that of an ideal gas. The upper graph shows how the reactive flux (green circles), defined as $\alpha_i(r_{\text{cut}}) \times \exp[-A_i(r_{\text{cut}})/k_{\text{B}}T]$, displays a well-defined minimum at the location of the dividing surface at $r_{\text{DNT}} = 2.8\,\text{Å}$, giving an evaporation rate constant $\alpha_2 = 160 \times 10^9\ \text{s}^{-1}$. The estimate of the rate constant will, of course, depend on the interaction potential. For example, if the TIP4P [62] model is used $\alpha_2 = 35 \times 10^9\ \text{s}^{-1}$—more than a factor of four slower than the Dang-Chang result. This is not too surprising since the TIP4P water dimer is more binding than Dang-Chang by nearly -1.5 kcal/mol at their respective global minima.

Before discussing the application of DNT to water, it is important to provide a summary of how the cluster free energies A_i are calculated. The Finite Time Variational External Work method [63] has been developed [55] into a practical and efficient MC procedure for calculating cluster Helmholtz free energies. This method is particularly useful since it provides not only cluster Helmholtz free energies but also error estimates that can be systematically improved. In the External Work method the free energy is determined by an incremental summation of (1) the energy exchanged between the cluster and the heat bath, and (2) the variation in the cluster Hamiltonian. This method is an amalgam of concepts from Clausius [64], Helmholtz [65], Metropolis [66], and Schrödinger [67]. The key concept can be traced back to Schrödinger [67] who interpreted doing work on a system as being equivalent to changing the system Hamiltonian. From the first and second laws of thermodynamics it can be shown that a reversible free energy change is equivalent to the work done on the system.

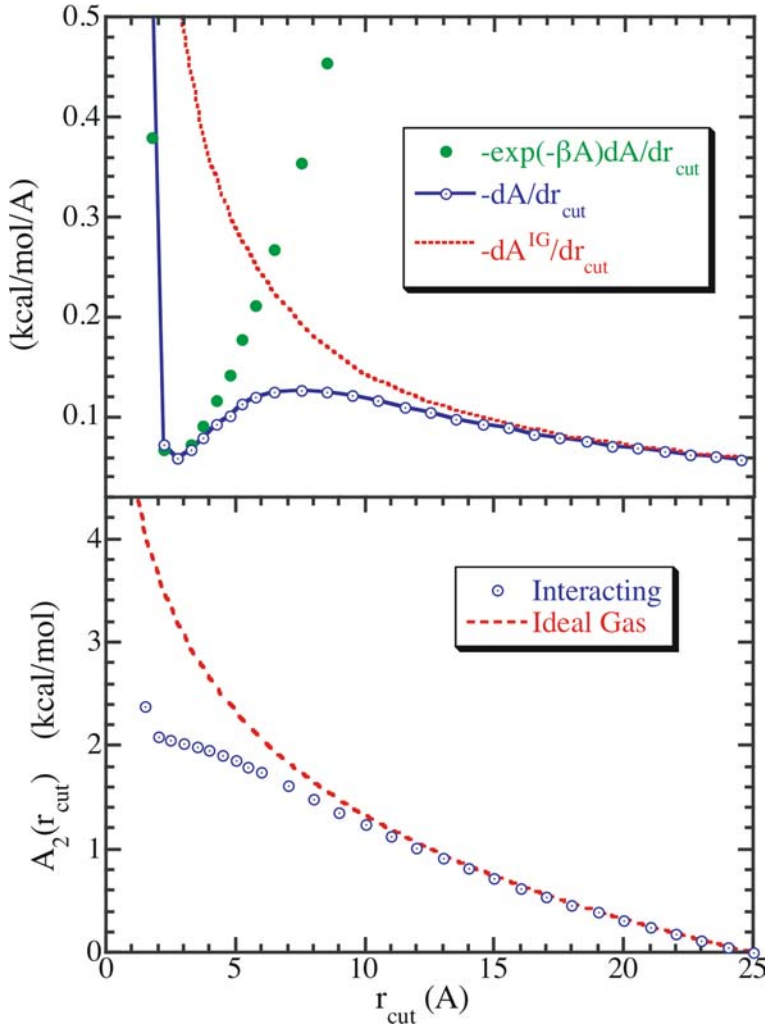

Fig. 4 Application of DNT to the Dang-Chang water dimer at 243 K. The lower graph shows the constraining radius dependence of the Helmholtz free energy and how for large r_{cut} the free energy approaches that of an ideal gas. The upper graph shows how the reactive flux (*green circles*) displays a well-defined minimum at the optimal location of the dividing surface $r_{\mathrm{DNT}} = 2.8\,\text{Å}$ giving an evaporation rate constant $\alpha_2 = 160\times10^9\ \mathrm{s}^{-1}$

The anharmonic free energy difference calculated is shown in Fig. 5 and represents the free energy between a convenient reference state (an ideal gas, $U = 0$) and a desired state (a fully interacting system, $U = U(\mathbf{r}^i)$) calculated at some convenient value of the constraining radius r_{cut}. The total cluster Helmholtz free energy is obtained by summing the free energies of the interacting cluster and the ideal gas cluster. Cluster free energies were obtained at $T = 243$ K, sampling 10–100's of millions of MC steps, yielding a statistical uncertainty of 0.5 kcal/mol.

As an example, we show the classical *anharmonic* free energy differences for Dang-Chang water clusters compared to the classical and quantum *harmonic* results in Fig. 6. From Fig. 6 it is seen that *anharmonic* effects on the partition function are extremely important when trying to understand the thermodynamic stability of nucleating clusters. The harmonic approximation is often employed [68] when trying to predict atmospherically relevant nucleation mechanisms, however, our work has shown that caution should be exercised before placing much weight on such approximations. Otherwise, one might be lead to conclude that even highly accurate electronic structure calculations are in error or that impurities are to blame when the real reason is simply inadequate statistical mechanical sampling of the *anharmonic* regions of the potential.

5 Application of DNT to water

We have used DNT to predict the nucleation rates for H_2O at $T = 243$ K using the Dang-Chang [61] interaction potential. The theoretical results in Fig. 7 compare quite well with the experiments of Strey et al. [69] using a Two-Piston Expansion Chamber and Mikheev et al. [21, 70] using a laminar flow tube reactor (LFTR). In order to achieve quantitative agreement with the experimental nucleation rates, the chemical potentials for the water clusters were all shifted uniformly by -0.3 kcal/mol. A systematic shift of the Dang-Chang

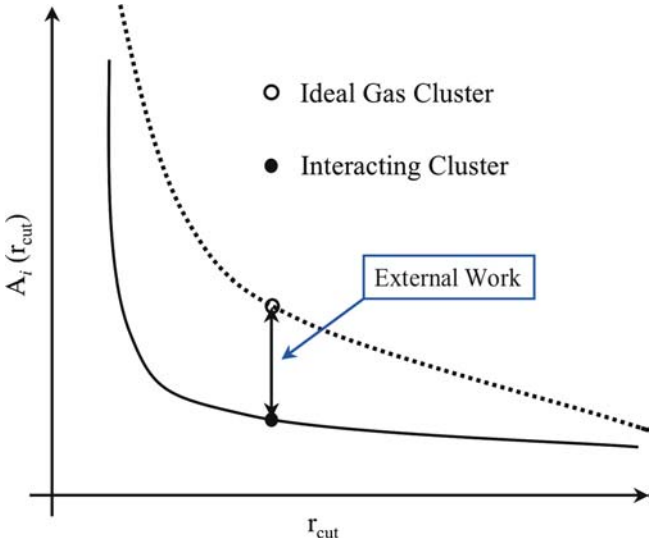

Fig. 5 Illustration of the finite external work method. The lower *solid curve* represents the dependence of the fully interacting *i*-cluster Helmholtz free energy on the constraining radius r_{cut}. The *upper dotted curve* represents the same dependence, however, the interactions are set to zero. The calculated external work is simply the free energy difference between the interacting and ideal gas *i*-clusters at some convenient value of r_{cut}

chemical potentials is justified by fundamental considerations of zero-point-energy (ZPE) effects on the cluster energies when compared to Feynman path integral simulation on interaction potentials fit to highly accurate electronic structure ground state energies [42]. This is an important issue because the Dang-Chang water potential was parameterized to reproduce the bulk density and enthalpy of vaporization at 298 K and hence implicitly includes ZPE effects but not in the rigorous manner dictated by quantum statistical mechanics. It should be noted that the interaction energy of $(H_2O)_2$ is −5.0 kcal/mol [71]. The ZPE for the dimer is +2.1 kcal/mol, calculated via the harmonic approximation, yielding a ZPE-corrected interaction energy of −2.9 kcal/mol. The shift in chemical potentials ($\mu_{i,i-1} \equiv A_i - A_{i-1}$) required to obtain agreement with experimental nucleation rates is only 14.3% of the water dimer ZPE. Choosing another popular bulk water model like TIP4P does not remedy the situation either. At 243 K the deviation in chemical potentials between TIP4P and Dang-Chang models is about −1.8 kcal/mol for the dimer and about −1.1 kcal/mol for the decamer, respectively. Thus, to be absolutely quantitative in calculating nucleation rates, very accurate interaction potentials must be developed and quantum nuclear degrees of freedom taken into account.

In order to get a better handle on the sensitivity of nucleation energetics [55] we used a phenomenological model for the chemical potentials of water clusters by Dillmann-Meier [72] (DM). Figure 8 shows the evaporation and condensation rate constants for water at 243 K and $S = 10$. Assuming gas-kinetics for the condensation rate constants (red squares), evaporation rate constants (black circles) can be calculated from detailed balance using the DM chemical potentials. If the evaporation rate constants (black circles) are held fixed and the chemical potentials decreased uniformly for all clusters, then the condensation rates will increase. A −0.5 kcal/mol shift in the cluster chemical potentials (condensation rates for this case are blue triangles) increases the nucleation rate by ten orders of magnitude. The results in Fig. 8 underscore the extreme sensitivity of nucleation to the underlying interactions. The physical reason why nucleation is so sensitive can be understood intuitively. Since nucleation is a

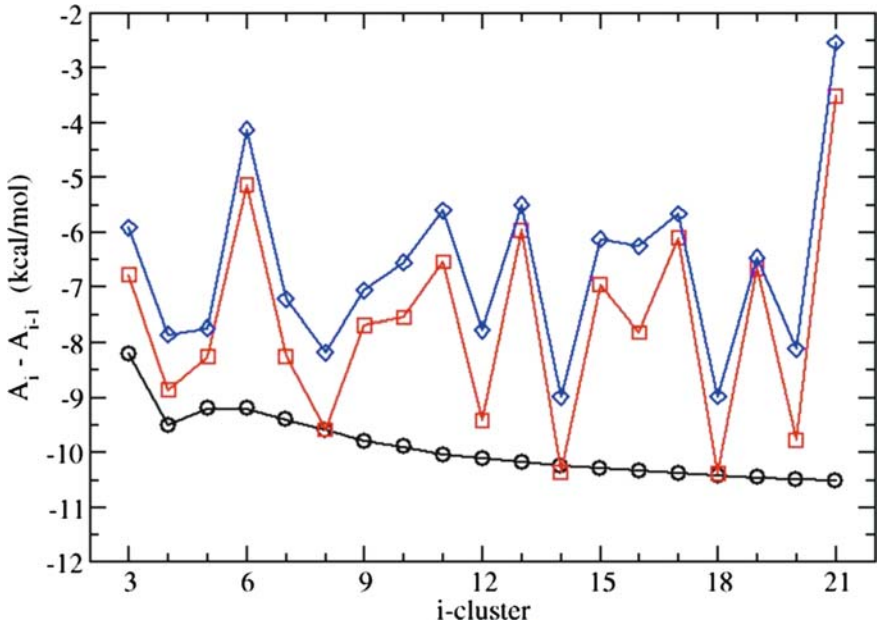

Fig. 6 Comparison of the classical anharmonic free energy differences (*black circles*) for Dang-Chang water clusters at 243 K compared to the classical (*red squares*) and quantum (*blue diamonds*) harmonic results. Clearly, the harmonic approximation is not so good

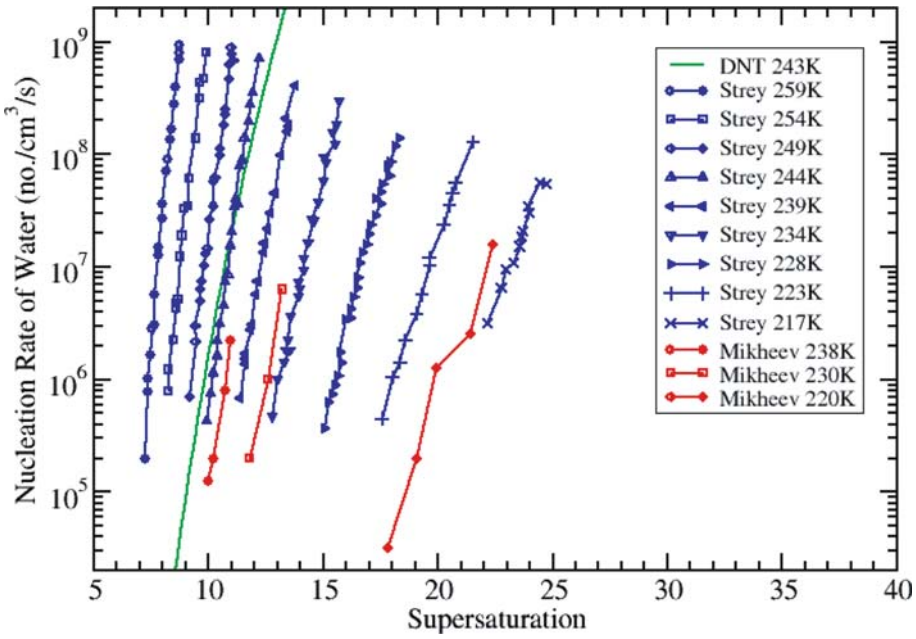

Fig. 7 Dynamical nucleation theory homogeneous nucleation rates for water at 243 K compared to experiment. The underlying *i*-cluster free energies were shifted by −0.3 kcal/mol to match experiment

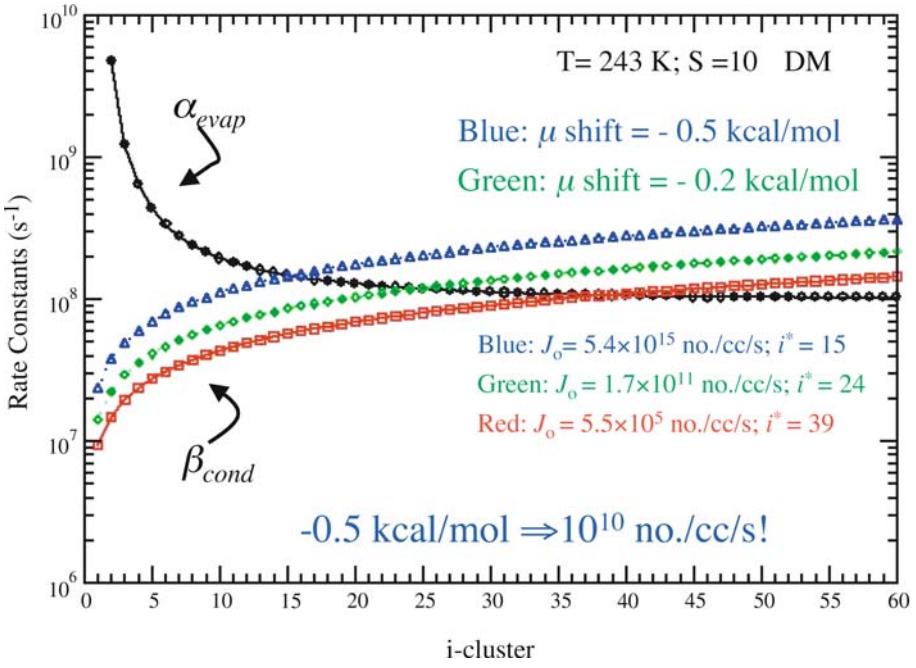

Fig. 8 Rate constants for DM water model assuming gas kinetics at T = 243 K and S = 10. The evaporation rate constants (*black circles*) are held constant while the lower curves are the condensation rate constants: (*red squares*) no change in chemical potentials, (*green diamonds*)—−0.2 kcal/mol shift in chemical potentials, (*blue triangles*) −0.5 kcal/mol change in chemical potentials. Notice that a −0.5 kcal/mol shift causes the nucleation rate to increase by ten orders of magnitude

multi-step chemical kinetics mechanism, small changes in each step can be amplified since there are so many reactions that must take place in order to reach the critical cluster. Stated another way, a 1 kcal/mol change in an Arrhenius activation barrier can change the rate constant by almost an order of magnitude. If this occurs over 40 or 50 reaction steps the consequences can be quite profound. The interested reader should see our previous publications for a more detailed discussion of sensitivity analysis for single and multi-component nucleation. In general, the more binding a potential is, the slower the evaporation rate constants will be for atoms or molecules trying to escape the clusters. A more binding

potential will also enhance the condensation rate constants by increasing the effective collision cross-section. Furthermore, if a trace contaminant interacts more favorably with the host nucleating vapor than the vapor does with itself, the clusters will preferentially form on the contaminants. Thus, all chemical interactions (e.g., hydrogen bonds, polar, nonpolar, radicals, ions, organics, inorganics, metals, solvated electrons, etc.) between cluster molecules must be accurately accounted for before the predictions are made. This should also be the case for heterogeneous nucleation on defects, vacancies, steps, edges, etc.

6 Extension of DNT to crystalization in solution

Crystallization in solution is one of the most challenging problems in chemical physics. Several atomistic studies of crystallization from the melt have been reported [52,73]. However, just a few simulations studying crystallization from solution have been published [74,75]. At a given temperature and pressure, solubility is defined as the concentration of a saturated salt solution in equilibrium with the salt precipitate—when this concentration is achieved the chemical potentials of the solute in solution and the pure salt crystallites are equivalent. A good example of how molecular simulations can provide insight into salt solubility is the investigation of aqueous KF solutions by Ferrario et al. [76]. The driving force for salt crystallization in solution occurs when the actual solute concentration exceeds the solution solubility (sometimes referred to as supersaturation). Salts having large solubilities require larger salt concentrations to crystallize than salts with lower solubilities. Anwar et al. [74] studied crystallization of Lennard-Jones (LJ) atoms from an LJ solvent at various supersaturations with and without a nucleation inhibitor. The results of their simulations were consistent with the experimental observation that increasing the supersaturation caused earlier onset of nucleation and that the presence of inhibitors retards the onset of nucleation. Furthermore, they found that nucleation from highly supersaturated solutions occur via liquid–liquid phase separation followed by solute nucleation. This work showed that the observed nucleation trends could be mimicked with the simplistic LJ models for solute/solvent. The recent work of Mucha and Jungwirth [75] simulated NaCl crystallization from an evaporating aqueous solution. Although interesting, their simulations do not capture the nucleation event within solution per se, but rather how NaCl ions group together as water leaves the system entirely. These studies displayed the ability of computer simulations to provide insight into crystallization; however, they were more characteristic of experiments rather than fundamental molecular-level theories of nucleation.

The relevant timescale for the nucleation event in solution is dictated by the potentials of mean force via the thermodynamic and kinetic properties of the clusters. This is particularly useful since nucleation is inherently a rare occurrence and trying to observe these events directly during a simulation at realistic conditions is very demanding computationally—major time is spent searching irrelevant regions of the solution configuration space. We present here a preliminary example of how to calculate the rate of salt cluster dissolution directly. Smith and Dang [77] used explicit solvent MD simulations to determine the potential of mean force (PMF) between Na^+ and Cl^- atoms in SPC/E water at 300 K. We can define the configurational partition function of the NaCl dimer by

$$Q(r_{\text{cut}}, T) = \int_0^{r_{\text{cut}}} \mathrm{d}r r^2 \exp[-W(r)/k_{\text{B}}T] = \exp[-A_{\text{Na-Cl}}(r_{\text{cut}}, T)/k_{\text{B}}T], \quad (17)$$

where $W(r)$ is the NaCl PMF in SPC/E water, $r = R_{\text{Na-Cl}}$ is the distance between the two ions, and $A_{\text{Na-Cl}}(r_{\text{cut}}, T)$ is the Helmholtz free energy of the aqueous NaCl dimer. The derivative of the salt dimer free energy with respect to r is

$$\left.\frac{\mathrm{d}A_{\text{Na-Cl}}}{\mathrm{d}r}\right|_{r=r_{\text{DNT}}} = -k_{\text{B}}T\left[\frac{1}{Q}\frac{\mathrm{d}Q}{\mathrm{d}r}\right]_{r=r_{\text{DNT}}}, \quad (18)$$

and

$$\left.\frac{\mathrm{d}Q}{\mathrm{d}r}\right|_{r=r_{\text{DNT}}} = \frac{\mathrm{d}}{\mathrm{d}r}\left[\int_0^{r_{\text{cut}}} \mathrm{d}r r^2 \exp[-W(r)/k_{\text{B}}T]\right]_{r=r_{\text{DNT}}} = r_{\text{DNT}}^2 \exp[-W(r_{\text{DNT}})/k_{\text{B}}T]. \quad (19)$$

Combining Eqs. 18 and 19 we obtain

$$\left.\frac{\mathrm{d}A_{\text{Na-Cl}}}{\mathrm{d}r}\right|_{r_{\text{DNT}}} = -k_{\text{B}}T\frac{r_{\text{DNT}}^2 \exp[-W(r_{\text{DNT}})/k_{\text{B}}T]}{\int_0^{r_{\text{DNT}}} \mathrm{d}r r^2 \exp[-W(r)/k_{\text{B}}T]}. \quad (20)$$

Using the result from Eq. 10 and Eq. 20 we obtain the NaCl dissolution rate

$$\alpha_{\text{Na-Cl}}(T) = -\frac{1}{\sqrt{2\pi\mu k_{\text{B}}T}}\left.\frac{\mathrm{d}A_{\text{Na-Cl}}}{\mathrm{d}r}\right|_{r_{\text{DNT}}} = \sqrt{\frac{k_{\text{B}}T}{2\pi\mu}}\frac{r_{\text{DNT}}^2 \exp[-W(r_{\text{DNT}})/k_{\text{B}}T]}{\int_0^{r_{\text{DNT}}} \mathrm{d}r r^2 \exp[-W(r)/k_{\text{B}}T]}, \quad (21)$$

where μ is the reduced mass of NaCl. This final result shows the equivalence between DNT and the transition state theory rate expression for reaction in solution derived by Hynes [78] for the special case of the NaCl dimer. The PMF for NaCl in SPC/E water at 300 K is shown in Fig. 9 as a function of the ion separation distance $R_{\text{Na-Cl}}$. The first minimum at 2.9 Å is the contact-ion pair (CIP) and the second minimum at 4.9 Å is the solvent-separated-ion pair (SSIP). Using Eq. 21, the DNT dissolution rate for the CIP is $\alpha_{\text{CIP}} \sim 0.3\,\text{ps}^{-1}$ with a PMF barrier of 1.9 kcal/mol and $\alpha_{\text{SSIP}} \sim 1.7\,\text{ps}^{-1}$ with a PMF barrier of 0.6 kcal/mol. The result for the CIP dissolution rate agrees with the Smith and Dang result of $0.29\,\text{ps}^{-1}$, as it should. However, they did not calculate the SSIP dissolution rate for comparison. It should be noted that Smith and Dang found that solvent induced recrossing effects were important and reduced the dissolution rate for the CIP by a factor of six. Moreover, they found differences between the NaCl PMFs in SPC/E and RPOL water models. In particular, the positions of the SSIP minimum were shifted with the RPOL SSIP barrier less well defined. This preliminary study gives us hope

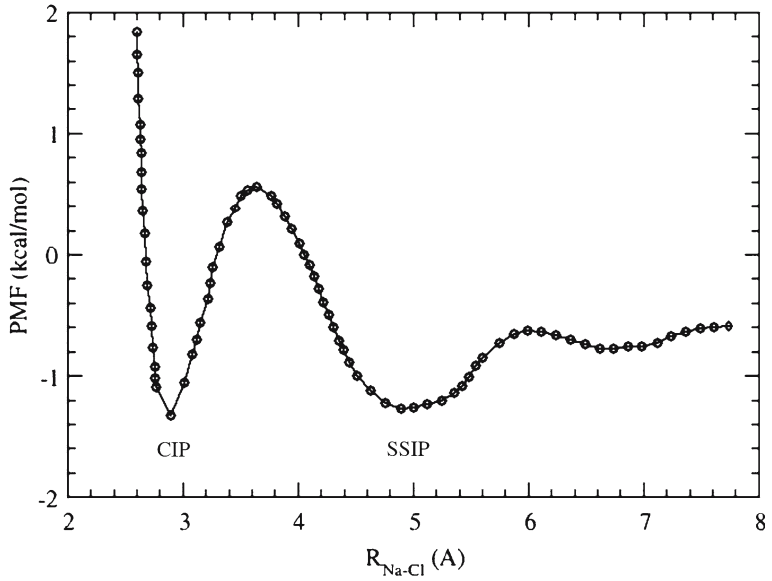

Fig. 9 The PMF for NaCl in SPC/E water at 300 K as a function of the ion separation distance R_{Na-Cl}. The first minimum at 2.9 Å is the contact-ion pair (CIP) and the second minimum at 4.9 Å is the solvent-separated-ion pair ($SSIP$). The DNT dissolution rate for the CIP is $\alpha_{CIP} \approx 0.3\,ps^{-1}$ with a PMF barrier of 1.9 kcal/mol and $\alpha_{SSIP} \approx 1.7\,ps^{-1}$ with a PMF barrier of 0.6 kcal/mol

that extending DNT to salt crystallization in aqueous solution will be fruitful, however, more general dividing surfaces will probably be required to capture the various dissolution channels.

7 Comments and conclusions

Dynamical nucleation theory is a molecular-level treatment of nucleation kinetics based upon variational transition state theory to obtain rate and equilibrium constants for the clustering reactions involved in phase transformations. DNT requires accurate cluster free energies and rate constants. In order to predict nucleation rates quantitatively, cluster properties must be determined using accurate representations of the interactions. The details concerning the construction of interaction potentials and to what end they are used must be approached cautiously. Tenths of a kcal/mol accuracy in the interaction potentials and anharmonic statistical mechanical sampling represents a daunting challenge to computational chemistry if we are to understand and predict nucleation rates quantitatively. Currently, given the extreme sensitivity of nucleation to cluster interaction potentials, emphasis should be placed on understanding relative effects instead of absolute nucleation rates.

In summary, a fundamental understanding of chemical physics of nucleation will provide the insight, theoretical formalism, computational methodologies, and analysis for further application in many scientific endeavors (atmospheric sciences, chemistry, biology, nano-materials, trace chemical detection, etc.) and the ability to explore the effect of interactions, and conditions (temperature, solubility, pressure, electromagnetic fields, acoustic waves, etc.) on nucleation. The beneficial impacts of understanding nucleation are ubiquitous: materials and manufacturing, information technology, medicine and health, environment and energy, aeronautics and space exploration, and national security.

Acknowledgements I would like to acknowledge the help I received from several of my co-workers who provided useful insight and encouraged my research toward understanding nucleation: Gregory K. Schenter, Bruce C. Garrett, Nels S. Laulainen, Vladimir B. Mikheev, Stephan E. Barlow, Liem X. Dang, René L. Corrales, and Sotiris S. Xantheas. This work was supported in part by the Computational Science & Engineering LDRD Program at PNNL, and the Division of Chemical Sciences, Basic Energy Sciences, of the U.S. Department of Energy (DOE). This research was performed in part using the Molecular Science Computing Facility in the William R. Wiley Environmental Molecular Sciences Laboratory a national scientific user facility sponsored by the DOE's Office of Biological and Environmental Research and located at PNNL. Battelle operates the PNNL for DOE.

References

1. Fahrenheit DG (1724) Philos Trans Roy Soc 39:78
2. Lowitz JT (1795) Crells Chemische Annalen 1:3
3. Laplace P (1806) Traite de Mechanique Celeste 4; von Helmholtz R (1886) Ann Physik 27:508
4. Gay-Lussac JL (1813) Ann de Chimie 87:225
5. Pasteur L (1848) Ann Chim Phys. 24:442
6. Gernez D (1866) Compt Rend 63:843
7. Gibbs JW (1876) Trans Connect Acad 3:108
8. Coulier PJ (1875) J de Pharmacie et de Chemie 22:165
9. Aitken J (1880) Proc Roy Soc 11:14
10. Wilson CTR (1897) Trans Roy Soc (London) A189:265; Wilson CTR (1900) Trans Roy Soc (London) A193:289
11. Ostwald W (1896-1902) Lehrbuch Allgem. Chem., W. Engelmann, Leiprig, II, 2.
12. Volmer M, Weber A (1926) Z Phys Chem 119:277
13. Volmer M (1939) Kinetik der Phasenbildung. Theodor Steinkopff Verlag, Dresden

14. Farkas L (1927) Z Phys Chem A125:236
15. Becker R, Doering W (1935) Ann Phys 24:719; Becker R (1949) Discuss Faraday Soc 5:55
16. Band W (1939) J Chem Phys 6:654
17. Frenkel J (1939) J Chem Phys 7:200; Frenkel J (1955) Kinetic theory of liquids. Dover, New York
18. Gernez D (1865) Compt Rend 60:833
19. Arrhenius S (1889) Z Phys Chem 4:226
20. Ostwald WF (1897) Z Physik Chem Leipzig 22:289
21. Mikheev VB, Irving PM, Laulainen NS, Barlow SE, Pervukhin VV (2002) J Chem Phys 116:10772
22. Sioutas C, McMurry PH, Biswas P, Hinds WC, Wilson WE (2004) J Nanoparticle Res 6:319; Voisin D, Smith JN, Sakurai H, McMurry PH, Eisele FL (2003) Aerosol Sci Technol 37:471; Smith JN, Moore KF, McMurry PH, Eisele FL (2004) Aerosol Sci Technol 38:100
23. Mullins WW, Sekerka RF (1963) J Appl Phys 34:323
24. Mullins WW, Sekerka RF (1964) J Appl Phys 35:444
25. Berg WF (1938) Proc Roy Soc A 164:79
26. Langer JS (1980) Rev Mod Phys 52:1
27. Caroli B, Caroli C, Roulet B (1992) Instabilities of planar solidification front, in Solids far from Equilibrium. Cambridge University Press, Cambridge
28. Zettlemoyer AC (1969) Nucleation. Marcel Dekker, New York; Abraham FF (1974) Homogeneous nucleation theory. Academic, New York
29. Manna L, Milliron DJ, Meisel A, Scher EC, Alivisatos AP (2003) Nat Mater 2:382; Manna L, Scher EC, Alivisatos AP (2000) J Am Chem Soc 122:12700
30. Zeldovich J (1942) J Exp Theor Phys 12:525
31. Kulmala M, Korhonen P, Napari I, Karlsson A, Berresheim H, O'Dowd CD (2002) J Geophys Res 107:8111
32. Kulmala M, Vehkamaki H, Petaja T, Dal Maso M, Lauri A, Kerminen VM, Birmili W, McMurry PH (2004) J Aerosol Sci 35:143
33. Allen MP, Tildesley DJ (1987) Computer simulation of liquids. Oxford University Press, New York
34. Frenkel D (1993): In van Gunsteren WF, Weiner PK, Wilkinson AJ (ed) Computer simulation of biomolecular systems: theoretical and experimental applications, vol 2. ESCOM, Leiden, The Netherlands, p 37; Frenkel D, Smit B (1996) Understanding molecular simulation: from algorithms to applications. Academic, San Diego
35. Lee JK, Barker JA, Abraham FF (1973) J Chem Phys 58:3166
36. Kathmann SM, Hale BN (2001) J Phys Chem B 105:11719
37. Hale BN (1996) Aust J Phys 49:425; Kusaka I, Wang Z-G, Seinfeld JH (1998) J Chem Phys 108:3416
38. Kusaka I, Oxtoby D (1999) J Chem Phys 110:5249
39. Kusaka I, Wang Z, Seinfeld J (1995) J Chem Phys 103:8993; Kusaka I, Wang Z, Seinfeld J (1995) J Chem Phys 102:913; Kusaka I, Wang Z-G, Seinfeld JH (1998) J Chem Phys 108:6829; Kusaka I, Wang Z-G, Seinfeld JH (1998) J Chem Phys 108:3416; Oh K, Zeng X, Reiss H (1997) J Chem Phys 107:1242; Oh K, Zeng X (1999) J Chem Phys 110:4471; Schaaf P, Senger B, Reiss H (1997) J Phys Chem 101:8740; Schaaf P, Senger B, Voegel J-C, Reiss H (1999) Phys Rev E 60:771; Schaaf P, Senger B, Voegel JC, Bowles RK, Reiss H (2001) J Chem Phys 114:8091; Suzuki K (1996): In Kulmala M, Wagner PE (ed) Nucleation and atmospheric aerosols. Pergamon, New York; Senger B, Schaaf P, Corti D, Bowles R, Voegel J-C, Reiss H (1999) J Chem Phys 110:6421; Senger B, Schaaf P, Corti D, Bowles R, Pointu D, Voegel J-C, Reiss H (1999) J Chem Phys 110:6438
40. Schenter GK, Kathmann SM, Garrett BC (1999) Phys Rev Lett 82:3484; Schenter GK, Kathmann SM, Garrett BC (1999) J Chem Phys 110:7951
41. Schenter GK, Kathmann SM, Garrett BC (2002) J Chem Phys 116:4275
42. Schenter GK (2002) J Chem Phys 117:6573
43. Merikanto J, Vehkamaki H, Zapadinsky E (2004) J Chem Phys 121:914
44. Hale BN, Ward R (1982) J Stat Phys 28:487; Vehkamaki H, Ford IJ (1999) Phys Rev E 59:6483; Vehkamaki H, Ford IJ (2000) J Chem Phys 112:4193; Vehkamaki H, Ford IJ (2000) J Chem Phys 113:3261
45. Reiss H, Katz JL, Cohen ET (1968) J Chem Phys 48:5553; Reiss H, Tabazadeh A, Talbot J (1990) J Chem Phys 92:1266
46. Garcia N, Soler Torroja JM (1981) Phys Rev Lett 47:186
47. Debenedetti P, Reiss H (1998) J Chem Phys 108:5498; Debenedetti P, Reiss H (1999) J Chem Phys 111:3771
48. Stillinger FH (1963) J Chem Phys 38:1486
49. Yasuoka K, Matsumoto M (1998) J Chem Phys 109:8463
50. Zeng XC, Oxtoby DW (1991) J Chem Phys 95:5940; Zeng XC, Oxtoby DW (1991) J Chem Phys 94:4472; Laaksonen A, Talanquer V, Oxtoby DW (1995) Ann Rev of Phys Chem 46:489; Oxtoby DW (1992) J Phys: Condensed Matter 4:7627; Oxtoby DW, Evans R (1988) J Chem Phys 89:7521; Cahn JW, Hilliard JE (1959) J Chem Phys 31:688
51. ten Wolde P, Frenkel D (1998) J Chem Phys 109:9901; ten Wolde P, Ruiz-Montero M, Frenkel D (1999) J Chem Phys 110:1591
52. ten Wolde PR, Ruiz-Montero MJ, Frenkel D (1996) J Chem Phys 104:9932
53. Reiss, H (2004) In: Reiss H (ed) Critique of molecular theories of nucleation. AIP: Rolla, Missouri, Vol 534, pp 181
54. Kathmann SM, Schenter GK, Garrett BC (1999) J Chem Phys 111:4688
55. Kathmann SM, Schenter GK, Garrett BC (2002) J Chem Phys 116:5046
56. Kathmann SM, Schenter GK, Garrett BC (2004) J Chem Phys 120:9133
57. Kathmann SM, Schenter GK, Garrett BC (2005) Phys Rev Lett 94:116104
58. Heneghan AF, Wilson PW, Wang G, Haymet ADJ (2001) J Chem Phys 115:7599
59. Kathmann S, Schenter GK, Garrett BC (1999) J Chem Phys 111:4688
60. Ellerby HM (1994) Phys Rev E 49:4287; Ellerby HM, Weakliem CL, Reiss H (1991) J Chem Phys 95:9209; Ellerby HM, Weakliem CL, Reiss H (1992) J Chem Phys 97:5766; Weakleim CL, Reiss H (1993) J Chem Phys 99:5374; Weakliem CL, Reiss H (1994) J Chem Phys 101:2398
61. Dang LX, Chang T-M (1997) J Chem Phys 106:8149
62. Jorgensen WL, Chandrasekhar J, Madura JD, Impey RW, Klein ML (1983) J Chem Phys 79:926
63. Reinhardt WP, Hunter JE III (1992) J Chem Phys 97:1599; Reinhardt WP, Miller MA, Amon LM (2001) Acc Chem Res 34:607; Hunter III, JE, Reinhardt WP (1995) J Chem Phys 103:8627; Hunter III, JE, Reinhardt WP, Davis TF (1993) J Chem Phys 99:6856; Hogenson GJ, Reinhardt WP (1995) J Chem Phys 102:4151
64. Clausius R (1879) The mechanical theory of heat. MacMillan, London
65. Cahan D (1993) Hermann von Helmholtz and the foundations of nineteenth century science. University of California Press, Berkeley
66. Metropolis N, Rosenbluth AW, Rosenbluth MN, Teller AH, Teller E (1953) J Chem Phys 21:1087
67. Schrodinger E (1989) Statistical thermodynamics. Dover, NEW York
68. Vehkamaki H, Napari I, Kulmala M (2004) Phys Rev Lett 93:149501; Ianni J, Bandy AR (1999) J Phys Chem 103:2801; Ianni J, Bandy AR (2000) J Mol Struct 497:19; Re S, Osamura Y, Morokuma K (1999) J Phys Chem A 103:3535
69. Viisanen Y, Strey R, Reiss H (1993) J Chem Phys 99:4680; Viisanen Y, Strey R, Reiss H (2000) J Chem Phys 112:8205
70. Mikheev VB, Irving PM, Laulainen NS, Barlow SE, Pervukhin VV (2001) J Chem Phys 116:10772
71. Feyereisen MW, Feller DF, Dixon DA (1996) J Phys Chem 100:2993
72. Dillmann A, Meier GEA (1991) J Chem Phys 94:3872

73. Mandel MJ, McTague JP, Rahman A (1976) J Chem Phys 64:3699; Nose S, Yonezawa F (1986) J Chem Phys 84:1803; Esselink K, Hilbers PAJ, van Beest BWH (1994) J Chem Phys 101:9033; Huang J, Zhu X, Bartell LS (1998) J Phys Chem A 102:2708; Monson PA, Kofke DA (2000) Adv Chem Phys 115:113; Matsumoto M, Saito S, Ohmine I (2002) Nature 416:409
74. Anwar J, Boateng PK (1998) J Am Chem Soci 120:9600
75. Mucha M, Jungwirth P (2003) J Phys Chem B 107:8271
76. Ferrario M, Ciccotti G, Spohr E, Cartailler T, Turq P (2002) J Chem Phys 117:4947
77. Smith DE, Dang LX (1994) J Chem Phys 100:3757
78. Hynes JT (1985) The theory of chemical reaction dynamics. Chemical Rubber, Boca Raton